1. Jansky, K. *Proc. IRE* **20**, 1920 (1932).
2. Lynden-Bell, D. & Rees, M. J. *Mon. Not. R. astr. Soc.* **152**, 461–475 (1971).
3. Wollman, E. R., Geballe, T. R., Lacy, J. H., Townes, C. H. & Rank, D. M. *Astrophys. J.* **218**, L103–L107 (1977).
4. Krabbe, A., Genzel, R., Drapatz, S. & Rotaciuc, V. *Astrophys. J.* **382**, L19–L22 (1991).
5. Hauser, M. G. *et al.* NASA photograph G90-03046 (1990).
6. Hubble, E. *Astrophys. J.* **64**, 321–369 (1924).
7. de Vaucouleurs, G., in *IAU Symp. 20: The Galaxy and the Magellanic Clouds* (eds Kerr, F. J. & Rodgers, A. W.) 195–199 (Australian Academy of Science, Sydney 1964).
8. Peters, W. L. *Astrophys. J.* **195**, 617–629 (1975).
9. Liszt, H. S. & Burton, W. B. *Astrophys. J.* **236**, 779–797 (1980).
10. Yuan, C. *Astrophys. J.* **281**, 600–613 (1984).
11. Blitz, L. & Spergel, D. N. *Astrophys. J.* **379**, 631–638 (1991).
12. Matsumoto, T. *et al.* in *The Galactic Center* (eds G. Riegler & R. Blandford) 48–52 (American Institute of Physics, New York, 1982).
13. Weiland, J. *et al.* in *Back to the Galaxy* (ed. Verter, F.) (AIP, New York, in the press).
14. Weinberg, M. D. *Astrophys. J.* **384**, 81–94 (1992).
15. Nakada, Y. *et al. Nature* **353**, 140–141 (1992).
16. Whitelock, P. & Catchpole, R. in *The Center, Bulge and Disk of the Milky Way* (ed. Blitz, L.) 103–110 (Kluwer, Dordrecht, 1992).
17. Binney, J. J., Gerhard, O. E., Stark, A. A., Bally, J. & Uchida, K. I. *Mon. Not. R. astr. Soc.* **252**, 210–218 (1991).
18. Cohen, R. J. & Few, R. W. *Mon. Nat. R. astr. Soc.* **176**, 495–523 (1976).
19. Cohen, R. J. & Dent, W. R. F. in *Surveys of the Southern Galaxy* (eds Burton, W. B. & Israel, F. P.) 159–164 (Reidel, Dordrecht, 1983).
20. Bally, J., Stark, A. A., Wilson, R. W. & Henkel, C. *Astrophys. J. Suppl.* **65**, 13–82 (1987).
21. Contopoulos, G., & Mertzanides, C. *Astr. Astrophys.* **61**, 477–485 (1977).
22. Kent, S. M., Dame, T. M. & Fazio, G. *Astrophys. J.* **378**, 131–138 (1991).
23. Ciotti, L., D'Ercole, A., Pellegrini, S. & Renzini, A. *Astrophys. J.* **376**, 380–403 (1991).
24. Heiles, C. *Astrophys. J.* **324**, 321–330 (1988).
25. Boulares, A. & Cox, D. P. *Astrophys. J.* **365**, 544–558 (1990).
26. Yamauchi, S. *et al. Astrophys. J.* **365**, 532–538 (1991).
27. Güsten, R. in *The Center of the Galaxy* (ed. Morris, M.) 89–106 (Kluwer, Dordrecht, 1989).
28. Morris, M., Yusef-Zadeh, F. & Chance, D. in *Birth and Infancy of Stars* (eds Lucas, R., Omont, A. & Stora, R.) 209 (Elsevier, Amsterdam, 1985).
29. Spergel, D. N. & Blitz, L. *Nature* **357**, 665–667 (1992).
30. Morris, M. in *The Center of the Galaxy* (ed. Morris, M.) 171–177 (Kluwer, Dordrecht, 1989).
31. Stark, A. A., Bally, J., Wilson, R. W. & Pound, M. W. in *The Center of the Galaxy* (ed. Morris, M.) 129–133 (Kluwer, Dordrecht, 1989).
32. Shlossman, I., Frenk, J. & Begelman, M. *Nature* **338**, 45–47 (1989).
33. Yusef-Zadeh, F., Morris, M. & Chance, D. *Nature* **310**, 557–561 (1984).
34. Sofue, Y. & Handa, T. *Nature* **310**, 568–569 (1984).
35. Balbus, S. A. & Hawley, J. F. *Astrophys. J.* **376**, 214–222 (1991).
36. Blandford, R. D. & Payne, D. R. *Mon. Nat. R. Astr. Soc.* **199**, 883–903 (1982).
37. Pudritz, R. E. & Norman, C. A. *Astrophys. J.* **301**, 571–586 (1986).
38. Sofue, Y., Reich, W. & Reich, P. *Astrophys. J.* **341**, L47–L49 (1989).
39. Blitz, L., Bloemen, J. B. G. M., Hermsen, W. & Bania, T. M. *Astrophys.* **143**, 267–273 (1985).
40. Pedlar, A. *et al. Astrophys. J.* **342**, 769–784 (1989).
41. Genzel, R. in *The Center of the Galaxy* (ed. Morris, M.) 393–405 (Kluwer, Dordrecht, 1989).
42. Güsten, R. *et al. Astrophys. J.* **318**, 124–138 (1987).
43. Jackson, J. M. *et al. Astrophys. J.* **402**, 173–184 (1993).
44. McGinn, M. T., Sellgren, K., Becklin, E. E. & Hall, D. N. B. *Astrophys. J.* **338**, 824–840 (1989).
45. Ekers, R. D., van Gorkom, J. H., Schwarz, U. J. & Goss, W. M. *Astr. Astrophys.* **122**, 143–150 (1983).
46. Lo, K. Y. & Claussen, M. *Nature* **306**, 647–651 (1983).
47. Lacy, J. H., Geballe, T. R. & Hollenbach, D. J. *Astrophys. J.* **262**, 120–134 (1980).
48. Roberts, D. A., Goss, W. M. & van Gorkom, J. H. *Astrophys. J.* **366**, L15–L18 (1991).
49. Quinn, P. J. & Sussman, G. J. *Astrophys. J.* **288**, 377–384 (1985).
50. Serabyn, E. & Lacy, J. H. *Astrophys. J.* **293**, 445–458 (1985).
51. Aitkin, D. K., Gezari, D., Smith, C. H. McCaughrean, M. & Roche, P. F. *Astrophys. J.* **380**, 419–428 (1991).
52. Killeen, N. E. B., Lo, K. Y. & Crutcher, R. *Astrophys. J.* **385**, 585–603 (1992).
53. Ho, P. T. P. *et al. Nature* **350**, 309–312 (1991).
54. Okumura, S. K. *et al. Astrophys. J.* **378**, 127–130 (1991).
55. Mezger, P. G. *et al. Astrophys.* **209**, 337–348.
56. Zylka, R., Mezger, P. G. & Wink, J. *Astr. Astrophys.* **234**, 133–146 (1990).
57. Okumura, S. K. *et al. Astrophys. J.* **347**, 240–250 (1989).
58. Ho, P. T. P., Jackson, J. M., Barrett, A. H. & Armstrong, J. T. *Astrophys. J.* **288**, 575–579 (1985).
59. Szczepanski, J. C., Ho, P. T. P. & Güsten, R. in *Skylines, Proc. 3rd Haystack Observatory Mtg* (eds Haschick, A. D. & Ho, P. T. P.) 143–151 (Astr. Soc. Pacif., San Francisco, 1990).
60. Phinney, E. S. in *The Center of the Galaxy* (ed. Morris, M.) 543–553 (Kluwer, Dordrecht, 1989).
61. Sellgren, K., McGinn, M. T., Becklin, E. E. & Hall, D. N. B. *Astrophys. J.* **359**, 112–120 (1990).
62. Eckart, A. *et al. Nature* **355**, 526–528 (1992).
63. Allen, D. A., Hyland, A. R. & Hillier, D. J. *Mon. Nat. R. astr. Soc.* **244**, 706–713 (1990).
64. Adams, D. J. *et al. Astrophys. J.* **327**, L65–L68 (1988).
65. Rieke, G. H. & Lebofsky, M. J. in *The Galactic Center* (eds Riegler, G. R. & Blandford, R. D.) 194–302 (AIP, New York, 1982).
66. Gezari, D. Y. in *The Center, Bulge and Disk of the Milky Way* (ed. Blitz, L.) 23–46 (Kluwer, Dordrecht 1992).
67. Becklin, E. E., Gatley, I. & Werner, M. W. *Astrophys. J.* **258**, 135–142 (1982).
68. Werner, M. & Davidson, J. *IAU Symp.* No. 136, *The Center of the Galaxy* (ed. Morris, M.) 423–436 (Reidel, Dordrecht, 1989).
69. Balick, B. & Brown, R. L. *Astrophys. J.* **194**, 265–270 (1974).
70. Lo, K. Y., Backer, D., Kellerman, K., Moran, J. M. & Reid, M. *Nature* **315**, 124–125 (1985).
71. Rees, M. J. in *The Galactic Center* (eds Riegler, G. R. & Blandford, R. D.) 166–176 (AIP, New York, 1982).
72. Zylka, R., Mezger, P. G., & Lesch, L. *Astr. Astrophys.* **261**, 119–121 (1992).
73. Melia, F. *Astrophys. J.* **387**, L125–L28 (1992).
74. Reynolds, S. P. & McKee, C. F. *Astrophys. J.* **239**, 893–897 (1980).
75. Genzel, R. & Townes, C. H. *A. Rev. Astr. Astrophys.* **25**, 377–423 (1987).
76. Sanders, R. H. *Nature* **359**, 131–132 (1992).
77. Backer, D. & Sramek, R. *Abstr. URSI Mtg* (January 1993).
78. Haymes, R. C. *et al. Astrophys. J.* **201**, 593–602 (1975).
79. Riegler, G. R., Ling, J. C., Mahoney, W. A., Wheaten, W. A. & Jacobsen, A. S. *Astrophys. J.* **294**, L13–K15 (1985).
80. Leventhal, M., MacCallum, C. J., Husters, A. F. & Stang, P. D. *Astrophys. J.* **260**, L1–L5 (1982).
81. Lingenfelter, R. & Ramaty, R. in *AIP Proc.* No. 83 (eds Riegler, G. & Blandford, R.) 148–158 (American Institute of Physics, New York, 1982).
82. Bouchet, L. *et al. Astrophys. J.* **383**, L45–L48 (1991).

Ionospheric signatures of pulsed reconnection at the Earth's magnetopause

M. Lockwood*, W. F. Denig†, A. D. Farmer‡, V. N. Davda*, S. W. H. Cowley§ & H. Lühr‖

* Rutherford Appleton Laboratory, Chilton, Didcot OX11 0QX, UK
† Phillips Laboratory, PL/GPSG, Hanscom AFB, Bedford, Massachusetts 01731-5000, USA
‡ Atmospheric Physics Laboratory, University College London, London W1P 7PP, UK
§ Blackett Laboratory, Imperial College, London SW7 2BZ, UK
‖ Institut für Geophysik und Meteorologie, Technische Universität Braunschweig, W-3300 Braunschweig, Germany

THE plasma precipitating into the Earth's dayside auroral atmosphere has characteristics which show that it originates from the shocked solar-wind plasma of the magnetosheath[1,2]. The particles of the magnetosheath plasma precipitate down a funnel-shaped region (cusp) of open field lines resulting from reconnection of the geomagnetic field with the interplanetary magnetic field[3]. Although the cusp has long been considered a well defined spatial structure maintained by continuous reconnection, it has recently been suggested[4–6] that reconnection instead may take place in a series of discontinuous events; this is the 'pulsating cusp model'.

Here we present coordinated radar and satellite observations of a series of discrete, poleward-moving plasma structures that are consistent with the pulsating-cusp model.

Figure 1 shows schematically a noon–midnight cross-section of the Earth's magnetosphere, showing the cusps (C). The dashed line is the magnetopause, the current-carrying boundary between the magnetosphere and the shocked solar wind plasma in the magnetosheath (MS). The interplanetary magnetic field (IMF) is shown pointing southward, allowing it to reconnect with the northward-pointing 'closed' geomagnetic field lines(c) at a neutral line (X) in the subsolar magnetopause. This generates 'open' field lines (o) which thread the boundary and connect the magnetosphere with interplanetary space. The open field lines convect polewards under the joint action of magnetic 'tension' and the solar wind flow. If the rate at which field lines are reconnected exceeds the rate at which they convect polewards, the open/closed boundary migrates toward the Equator. Magnetosheath plasma can enter the magnetosphere along the open field lines. The large time-of-flight of the ions disperses them according to their energy[3]: highest-energy ions arrive first in the atmosphere and are seen at the lowest latitudes. This is because more recently reconnected field lines are always closer to the open/closed field line boundary which lies at the equatorward edge of the cusp[4].

If the reconnection were to take place at a steady rate, the ion energy would show a continuous latitudinal dispersion. However, the pulsating cusp model predicts that the dispersion
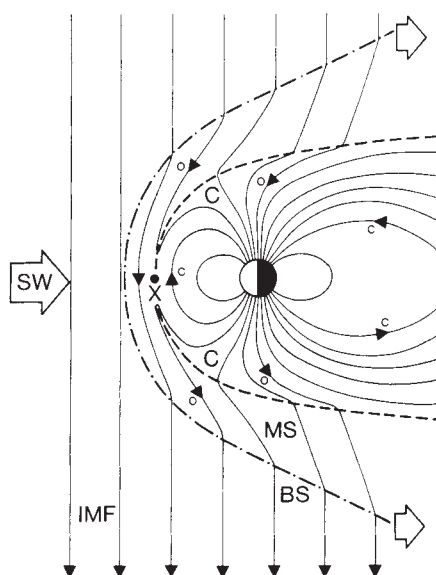
FIG. 1 Schematic of the dayside magnetosphere for southward interplanetary magnetic field (IMF). The super-Alfvénic solar wind (SW) forms a bow shock (BS), behind which lies the shocked plasma of the magnetosheath (MS). Reconnection takes place at X, converting closed field lines, c, into open field lines, o, which form a rotational field discontinuity where they cross the magnetopause (dashed line). This results in the open field lines convecting polewards under the magnetic 'tension' force, and in doing so they accelerate the magnetosheath ions that flow along them and cross the magnetopause[20,23]. As they straighten, open field lines continue to convect polewards because they are embedded in the solar wind flow, but the ion acceleration decreases (and turns to a deceleration poleward of the magnetic cusp). If the IMF has a significant dawn/duskward B_y component (out of the plane of the diagram), magnetic tension also causes east/west motion on the most recently reconnected field lines[6,17,19]. The injected magnetosheath plasma precipitates down the convecting open field lines, into the ionosphere in the cusps (C). The 'pulsating cusp' model[6,7,10] uses the fact that the spectra of particles arriving at the ionosphere on a given field line depend upon the time elapsed since that field line was reconnected. Ions with the lowest energy (E) observed on any one field line have the longest time-of-flight, t, and were therefore the first injected: they crossed the magnetopause at X, a distance d from the satellite ($t = d \, (2E/m_i)^{-1/2}$, where m_i is the ion mass). That minimum energy falls with time elapsed since reconnection. Hence two pulses of reconnection, with an interval δt between them, cause a step in the minimum energy from E_1 to E_2 where $\delta t = (t_2 - t_1) = d \, (m_i/2)^{1/2}(E_2^{-1/2} - E_1^{-1/2})$.
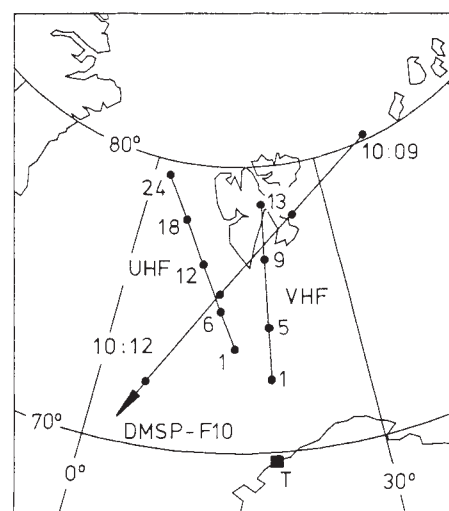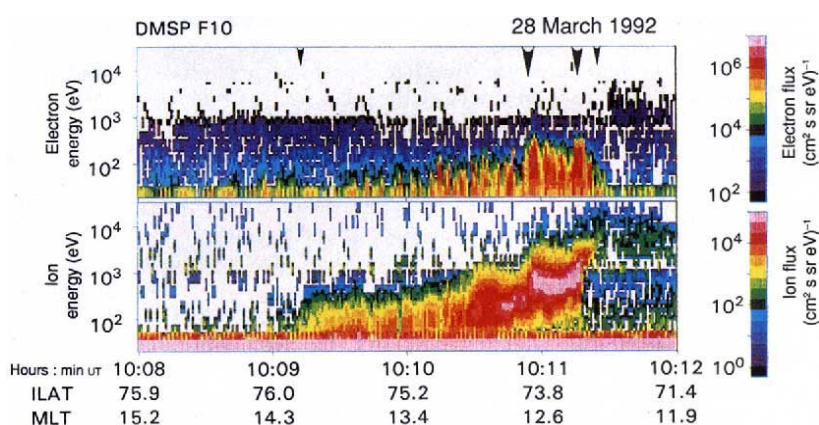

FIG. 2 Map (geographic coordinates) of the EISCAT UHF and VHF radar beams for the SP-UK-CONV experiment, used to study the ionized upper atmosphere in the F-region ionosphere on 28 March 1992: the points show centres of the radar range gates. The altitude of the UHF radar beam varies from 197 km for gate 1 to 595 km for gate 25. Also shown is the path of the DMSP-F10 satellite between 10:09 and 10:12 UT. The satellite passed at 800 km altitude over the EISCAT field-of-view, observing the same field line as the UHF radar at 10:11 UT. In magnetic coordinates, both were then at 12:55 magnetic local time (MLT) and an invariant (magnetic) latitude of $\Lambda = 74°$. Invariant latitude is a way of defining a magnetic field line by the motion of energetic charged particles along it and is the magnetic latitude of the point where the field line intersects the Earth. MLT is defined in terms of the point where the field line would cut the ecliptic plane and the angle that point subtends with the Sun at the Earth's centre. That angle is zero at MLT = 12 hr and cusp precipitation is generally found at MLT between 10:30 and 13:30 (ref. 12). Magnetic coordinates of both the radar range gates and the satellite position were determined using the IGRF (International Geomagnetic Reference Field) model of the Earth's magnetic field.

FIG. 3 Spectrograms showing the differential number flux (in $\text{cm}^{-2} \text{s}^{-1} \text{sr}^{-1} \text{eV}^{-1}$) of precipitating electrons (top) and ions (bottom) as a function of energy and time, as observed by DMSP-F10 during the pass described in Fig. 2. The decrease of ion energies with latitude at all times (and the observed convection away from the Sun) indicates that the IMF points southward; inverse-slope, V-shaped or dispersionless signatures are expected for northward IMF[3,6,14]. The arrows mark the boundaries of the 'cusp' (between larger arrows), 'cleft' and 'mantle' precipitations (equatorward and poleward of the cusp, respectively). The cusp–cleft boundary is defined to be where the mean ion energy falls below 3 keV (refs 1, 12), and the cusp–mantle boundary where the ion energy flux falls below $10^{10} \text{ eV cm}^{-2} \text{s}^{-1} \text{sr}^{-1}$. The electron energy flux in the cusp averages $3 \times 10^{10} \text{ eV cm}^{-2} \text{s}^{-1} \text{sr}^{-1}$, which is a factor of two lower than some definitions, under which this region would be classed as 'probably cusp'. However, this category shows the same statistical occurrence as 'cusp' (with electron energy flux exceeding $6 \times 10^{10} \text{ eV cm}^{-2} \text{s}^{-1} \text{sr}^{-1}$) (ref. 12). In the 'cleft', ions of energy up to a maximum of 5.5 keV (i.e. velocity of 1,000 km s^{-1}) are observed, revealing acceleration to above magnetosheath energies. This is the same as the peak field-aligned velocity of the D-shaped

distributions of the accelerated magnetosheath ions at the magnetopause, as both predicted theoretically[23] and, recently, observed[24-26]. This similarity indicates that the 'cleft' is, for this case at least, on the most-recently opened field lines: this is the only place where these highest-energy ions will be observed because of their low time-of-flight.
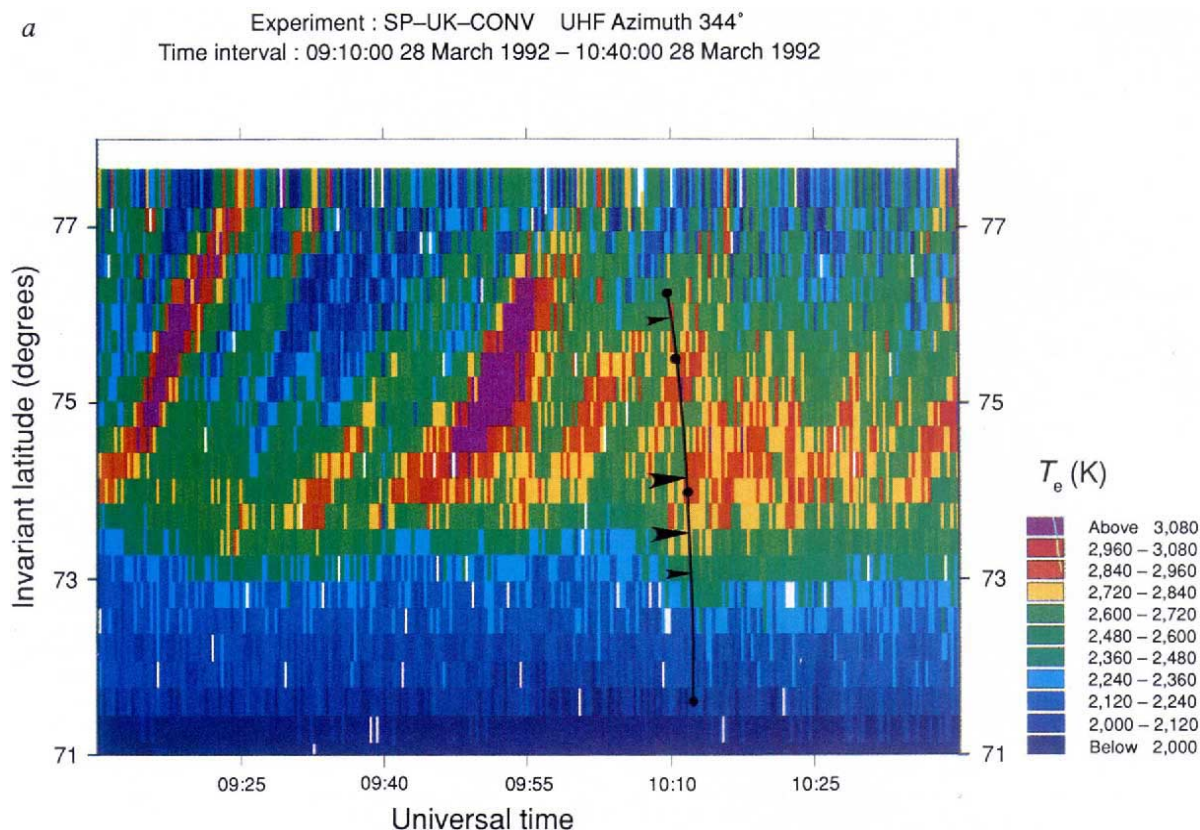
FIG. 4 The electron temperatures observed by the EISCAT UHF radar as a function of invariant latitude (Λ) and time for (a) extended and (b) short periods around the satellite pass. The Λ of the F10 satellite is given by the black line; dots are time markers 1 min apart; the outer small arrows are the edges of the observed magnetosheath-like plasma and the inner, large arrows mark the location of the two major step features in the ion dispersion signature (Fig. 3). At the time that magnetosheath-like ('mantle') precipitation is first observed, the satellite is at a MLT 1.6 hr further into the afternoon sector than the UHF radar beam at the same Λ (ΔMLT = +96 min), but at the edges of the 'cusp' (the larger arrows) ΔMLT is just +9 min and −6 min and at the equatorward edge of the 'cleft', it is −9 min. Hence for the cusp and cleft regions the satellite–radar conjunction is very close. In b we also

signature will show discontinuities if the reconnection is pulsed, rather than steady[6,7]. The ions appearing at the foot of the most recently reconnected field lines would be more energetic than the corresponding ions on field lines that were opened by a previous pulse of reconnection. Between these two regions, a step in the ion energy will be observed, corresponding to the period of little or no reconnection between the pulses. The steps will drift polewards with the convecting field lines.
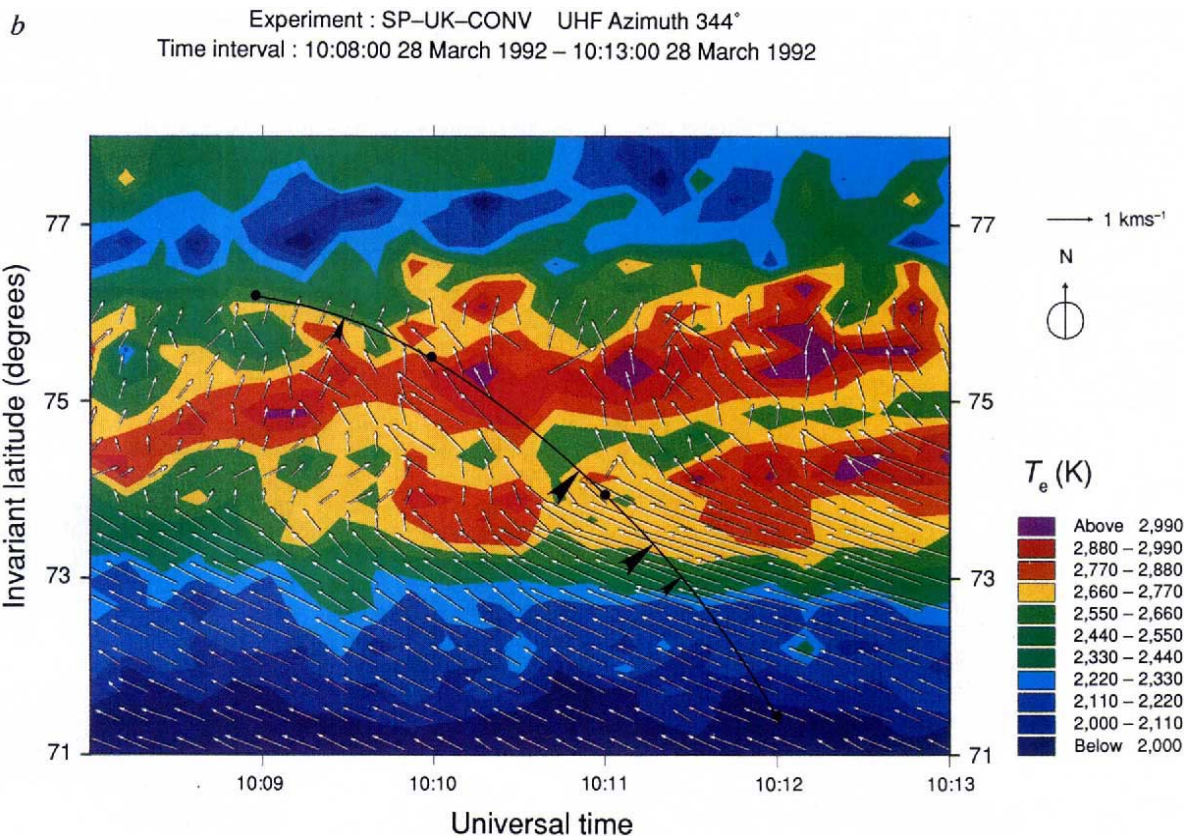
Such 'staircase' signatures are common in cusp ion precipitation[8,9] and have been used to calculate the reconnection rate as a function of time[10]. Hence the pulsating cusp model provides a powerful tool for studying how reconnection proceeds at the dayside magnetopause. However, there has been debate as to the validity of the model[11-13] with some scientists favouring the original explanation in terms of steady-state spatial structure[8,14], dividing the precipitating plasma into 'cleft', 'cusp' and 'mantle' regions[1,12].

Ambiguity between spatial and temporal variations is a common problem in interpreting any sequence of data from an orbiting satellite. Ground-based observations, on the other hand, offer an opportunity for remote sensing of the plasma in a given region over a prolonged period. Such measurements distinguish temporal events from spatial structure, but suffer from lower resolution. In the case of the cusp, we can detect transient features from the ground, but cannot unambiguously define them as being due to the cusp precipitation[15,16]. Here we report combined observations by the EISCAT radars and the DMSP-

F10 satellite which tell us about the spatial and temporal behaviour of the cusp. A map of the observations, made on 28 March 1992, is given in Fig. 2.

Figure 3 shows the energy–time spectrograms of the ions and electrons observed by the F10 satellite; magnetosheath-like plasma was observed between 10:09:15 and 10:11:30 UT. The most striking feature of these data is the ion-energy dispersion which showed discrete steps in the ion spectrum at 10:10:28, 10:10:54 and 10:11:15 UT. The electron fluxes were irregular, with peaks in the precipitating energy flux at the second and third of the steps which bound the 'cusp' precipitation: the regions polewards and equatorwards would usually be termed 'mantle' and 'cleft', respectively[1,12].

Figure 4 shows the electron temperature observed by the EISCAT ultra-high-frequency (UHF) radar as a function of invariant latitude, Λ (see Fig. 2), and time. The black line shows the Λ of the satellite for 10:09–10:12 UT, the arrows corresponding to those in Fig. 3. The large arrows mark the locations of two steps bounding the cusp, which were observed very near the UHF beam. The radar reveals a number of poleward-moving regions in which the electron temperature is elevated by a factor of ~1.5. The size, amplitude and repeat period of these events vary and those during the satellite pass are weaker than those seen just a few minutes earlier. These features are reminiscent of those observed in 630-nm dayside auroral emissions at winter solstice[15]. We expect heating of the ambient ionospheric electron gas in response to the precipitation of solar wind plasma[17], and the plasma density data (not shown) reveal that weak density

b

Experiment : SP–UK–CONV   UHF Azimuth 344°
Time interval : 10:08:00 28 March 1992 – 10:13:00 28 March 1992

show 10-s flow vectors, derived by combining the line-of-sight velocities from the UHF and VHF radars (where both are available). The satellite measured the component of the drift perpendicular to its orbit path and at all times for which a comparison could be made, this was the same (to within 10%) as that derived from the radar data. The UHF beam elevation is 20°, but we know altitude variations are not a major factor because (1) the same features were seen at the same time and Λ at greater altitudes by the VHF radar which employed an elevation of 30°; (2) low electron temperatures ($T_e < 2,200$ K) were observed polewards of the events; and (3) the features drifted polewards with the observed poleward component of the plasma convection. Hence the events are poleward-moving latitudinal structures and not rising, extensive, thin layers.

increases emerge within the events late in their lifetime, at the highest latitudes. This indicates that the events are caused by the low-energy particle precipitation and suggests that they may be involved in the production of polar cap density 'patches'[18]. The radar data alone cannot tell us that these features are indeed the cusp. However, Fig. 4b shows the data during the satellite overpass at higher time resolution and it can be seen that the southernmost event was coincident with the cusp (between the large arrows). A poleward-moving event is also seen in the mantle region. No temperature event is seen under the cleft precipitation in Fig. 4b, but 4a shows that this emerges as a third poleward-moving event after 10:14 UT. Using the theory outlined in Fig. 1 (ref. 10), the time interval δt (~5.3 min) between the events seen by EISCAT and the step in the lower cut-off of the ion energy seen by F10 (from $E_1 \approx 1.2$ keV to $E_2 \approx 200$ eV) yield a distance from the satellite to the neutral line (X in Fig. 1) of $d \approx 10^5$ km (16 Earth radii R_E). This places the reconnection close to the subsolar magnetopause, consistent with previous studies of both 'steady' reconnection[19,20] and 'flux transfer events' (FTEs)[21].

By combining the data from the two radars, convection vectors of 10-s resolution can be derived, with the assumption that the flow does not vary between the two beams. The results are also shown in Fig. 4b. At all times the poleward convection speed was ~500 m s⁻¹, the same as the speed of poleward drift of each of the heated regions as predicted by the pulsating cusp model. The flow rotates from uniformly northwestwards to northwards close to the poleward edge of the cusp. Hence the cusp was on

field lines which were convecting with similar velocity to the closed field lines equatorward of the cusp. This feature is predicted by the pulsating cusp model: a pulse of reconnection is envisaged as initially producing an equatorward motion of the open/closed boundary, rather than causing a burst of poleward flow (with the boundary static). This can excite continuous, even steady, poleward flow as the boundary subsequently relaxes poleward[4,6,7]. If the *y*-component of the interplanetary magnetic field $|B_y|$ were large, the tension force would yield a strong zonal flow burst on the most recently opened flux[6,7,16]: the moderate northwestward flow observed here in the cusp/cleft region implies that B_y is weakly positive; we cannot confirm this inference because no simultaneous measurements were made of the interplanetary magnetic field.

These results show that the magnetosheath-like plasma precipitation was, in fact, made up of three poleward-moving events from an extended sequence of such features. The satellite intersections with these three events would have been termed 'mantle', 'cusp' and 'cleft' in a spatial interpretation, but the radar shows them to be similar events seen at different phases of their evolution. This finding is supported by the steps in the dispersion signature of the ions. Hence the cusp was not, at this time at least, a steady-state spatial feature, but was one of a sequence of poleward-moving events. This is direct evidence for the pulsating cusp model and that reconnection was taking place in a series of bursts (FTEs) at the subsolar magnetopause. The period between the events which can be resolved in Fig. 4a varies between about 2 and 15 min. This is consistent with the

range for the magnetopause signatures which are also widely believed to result from FTEs[22]. □

1. Newell, P. T. & Meng, C.-I. *J. geophys. Res.* **93**, 14549–14556 (1988).
2. Heikkila, W. J. & Winningham, J. D. *J. geophys. Res.* **76**, 883–891 (1971).
3. Reiff, P. H. *et al. J. geophys. Res.* **82**, 479–491 (1977).
4. Lockwood, M. & Smith, M. F. *Geophys. Res. Lett.* **16**, 879–882 (1989).
5. Smith, M. F. & Lockwood, M. *Geophys. Res. Lett.* **17**, 1069–1072 (1990).
6. Smith, M. F. *et al. Planet. Space Sci.* **40**, 1251–1268 (1992).
7. Cowley, S. W. H. *et al.* in *CLUSTER-Dayside Polar Cusp, ESA SP-330*, (ed. Barron, C. I.) 105–112 (European Space Agency Publications, Nordvijk, The Netherlands, 1991).
8. Newell, P. T. & Meng, C. I. *Geophys. Res. Lett.* **18**, 1829–1832 (1991).
9. Escoubet, P. *et al. Geophys. Res. Lett.* **19**, 1735–1738 (1992).
10. Lockwood, M. & Smith, M. F. *J. geophys. Res.* **97**, 14841–14847 (1992).
11. Newell, P. T. *Geophys. Res. Lett.* **17**, 303–304 (1990).
12. Newell, P. T. & Meng, C.-I. *Geophys. Res. Lett.* **19**, 609–613 (1992).
13. Lockwood, M. & Smith, M. F. *Geophys. Res. Lett.* **17**, 305–306 (1990).
14. Lundin, R. *et al.* in *CLUSTER-Dayside Polar Cusp* (ed. Barron, C. I.) *ESA SP-330*, 83–95 (European Space Agency Publications, Nordvijk, The Netherlands, 1991).
15. Sandholt, P. E. *et al. Ann. Geophys.* **10**, 483–497 (1992).
16. Lockwood, M. *et al. Planet. Space Sci.* **37**, 1347–1365 (1989).
17. Curtis, S. A. *et al. Geophys. Res. Lett.* **9**, 997–1000 (1982).
18. Tsunoda, R. T. *Rev. Geophys.* **26**, 719–760 (1988).
19. Gosling, J. T. *et al. J. geophys. Res.* **95**, 8073–8084 (1990).
20. Paschmann, G. in *Magnetic Reconnection in Space and Laboratory Plasmas*, 114–123 (AGU Monogr. 30, 1984).
21. Russell, C. T. *et al. Adv. Space Res.* **5**, 363–369 (1985).
22. Lockwood, M. & Wild, M. N. *J. geophys. Res.* (in the press).
23. Cowley, S. W. H. *Rev. Geophys.* **20**, 531–565 (1982).
24. Smith, M. F. & Rodgers, D. J. *J. geophys. Res.* **95**, 11617–11624 (1991).
25. Fuselier, S. A. *et al. Geophys. Res. Lett.* **18**, 139–142 (1991).
26. Gosling, J. T. *et al. Geophys. Res. Lett.* **17**, 2245–2248 (1990).

Photochemical switching of polarization in ferroelectric liquid-crystal films

Tomiki Ikeda*, Takeo Sasaki & Kunihiro Ichimura

PRESTO, JRDC, Research Laboratory of Resources Utilization, Tokyo Institute of Technology, 4259 Nagatsuta, Midori-ku, Yokohama 227, Japan

LIQUID crystals have been used extensively as active media in display devices such as full-colour television screens. These devices are generally based on changes in the arrangement of the liquid-crystal molecules induced by electric fields, which change their optical properties[1]. Ferroelectric liquid crystals[2,3] exhibit spontaneous polarization and therefore show a faster response to changes in the applied field. Switching of this field causes a reversal in the direction of polarization[2–5]. Here we report polarization switching in ferroelectric liquid crystals driven by a photochemical process. The liquid-crystal films are doped with a photochromic compound which undergoes *trans–cis* isomerization on irradiation. Photoisomerization induces a change in the switching potential of the host liquid-crystal film, and thereby causes switching at the irradiated sites. The process is fast, stable, reversible and repeatable, and should be exploitable in device applications.

Many studies have been done on the photoresponse of liquid crystals (LCs), with an aim to developing optical image-recording systems[6–13]. Laser-addressed LC display devices have been demonstrated, based on the thermal control of LC alignment. In contrast to these 'heat-mode' systems, 'photon-mode' devices involve photochemical control and switching of alignment. Haas *et al.*[9] reported a change in selective reflectivity of a cholesteric LC mixture of cholesteryl bromide and other cholesteryl derivatives on photoirradiation, owing to a change

in the helical pitch of the cholesteric LC induced by a photochemical reaction of cholesteryl bromide. Photochemical reactions of guest molecules in LC hosts can induce a decrease of the nematic–isotropic phase transition temperature (T_{NI}) of the mixture and cause an isothermal phase transition at the irradiated sites[10–12]. Although such a photochemically induced phase transition might be exploited in optical image-recording systems, the response time and working temperature are disadvantageous. Time-resolved measurements[14,15] have revealed that the photochemical phase transition of low-molecular-weight or polymeric LCs takes place on a timescale of 50–200 ms. Furthermore, the temperature range is limited because the lowering of T_{NI} due to the photochemical reaction of the guest is generally small ($\leqslant 10$ °C). To achieve a quicker response and a wider temperature range for optical image recording systems, a different principle is needed.

The chiral smectic C (SmC*) phase of ferroelectric LCs (FLCs) exhibits spontaneous polarization (Ps), owing to the presence of polar groups which give the molecules an electric dipole moment. In the FLC **1**, dipole moments arising from the carbonyl moieties lie perpendicular to the long axis of the FLC molecules. In the SmC* phase, the FLC molecules are aligned parallel to each other to form a layer with a tilt between the direction of the long axis of the FLC molecule and the normal to the smectic layer[2,3]. The average direction of the molecular long axis (director, **n**) is defined in each layer, and owing to the chiral group in the FLC molecules the director adopts a helicoidal structure with a characteristic pitch. This means that
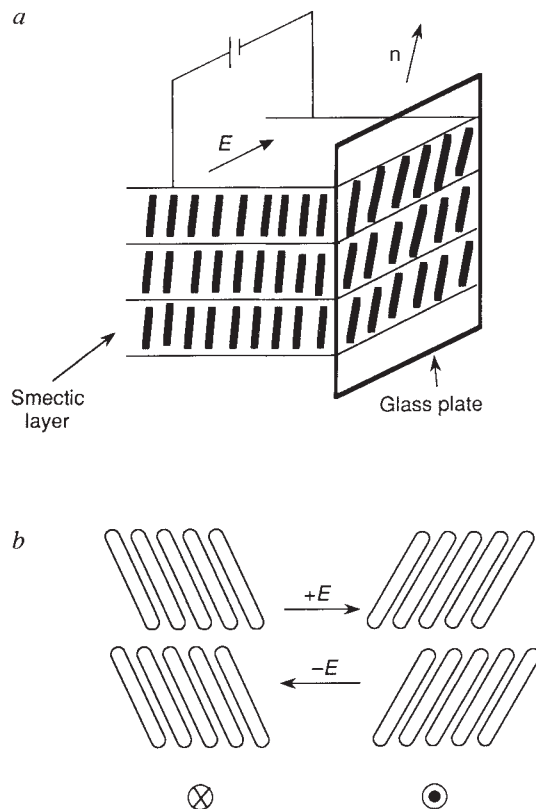

FIG. 1 Orientation of SmC* layers (*a*) and direction of spontaneous polarization (*b*) in the surface-stabilized state. In *a*, mesogens are aligned parallel to each other to form layers with a tilt between the director (**n**) and the normal to the smectic layer. The smectic layers are roughly perpendicular to the plates. The polarization can be made to reverse by applying an external electric field normal to the plane, which simultaneously causes the change in optical property of FLC. When viewed with a pair of polarizers, the right state transmits light while the left state extinguishes, thus producing a contrast between the two states.

* To whom correspondence should be addressed.